JOURNAL OF MATERIALS SCIENCE 36 (2001) 4511–4518

Structural features of $\Sigma = 19$, [110] GaAs tilt grain boundaries

N.-H. CHO*
Department of Materials Science and Engineering, Inha University, Inchon, Korea 402-751
E-mail: nhcho@inha.ac.kr

C. B. CARTER
Department of Chemical Engineering and Materials Science, University of Minnesota, MN, USA

$\Sigma = 19$, [110] tilt grain boundaries have been observed to facet parallel to particular planes; the facets lie along $(\bar{3}3\bar{1})_A/(3\bar{3}\bar{1})_B$, $(\bar{5}58)_A/7\bar{7}4)_B$ and $(\bar{2}2\bar{7})_A/(4\bar{4}5)_B$. The structural unit of the $\Sigma = 19$ $(\bar{3}3\bar{1})_A/(3\bar{3}\bar{1})_B$ [110] boundaries consists of 5- and 7-member rings, which are similar to the core structure of a/2[110] edge dislocations. The polarities in each grain on either side of the boundaries has been confirmed by CBED methods; a lower number of anti-site type cross-boundary bonds occur along the boundaries compared to when the polarity of one grain is reversed. The presence of 7-member rings and anti-site cross-boundary bonds results in a more open atomic structure at the boundary, shortening the distance between the first and the second {331} atomic planes from the boundary plane by 40%.

1. Introduction

As much attention has been focused on the correlation between structural defects and properties of materials, there has been an increasing amount of research carried out to obtain a greater understanding of grain boundaries. Over the last decade, semiconductor materials such as Si, Ge, and GaAs have become more important due to the use of these materials in manufacturing a variety of electronic devices.

Several theoretical and experimental studies have also been reported about tilt grain boundaries in fcc metal, and diamond-structure materials [1–4]. Theoretical calculations have been carried out to predict the relaxed atomic structure of these boundaries in such materials by using a particular interatomic potential at boundaries [5–7]. In particular, unlike grain boundaries in metals, the direction and length of the bonds across boundaries (cross-boundary bonds) were regarded as playing an important role in achieving a lower energy state of the boundaries in Ge or Si due to the strong directionality of covalent bonds. So far considerable attempts have been made to determine the atomic structure of grain boundaries in Ge and Si [8, 9]. However relatively little work has been carried out concerning the structure of grain boundaries in semiconductor materials with the sphalerite structure partly because of the difficulty of making particular boundaries. Epitaxial growth of thin film has been applied to make bicrystals in GaAs by reproducing the misorientation of substrates [10, 11]. The use of Ge bicrystals as substrates allows more control over the interface plane.

High-resolution imaging technique can be used in order to obtain information about the atomic sites near grain boundaries. Such observations have been successfully carried out on particular tilt grain boundaries with specific orientations in Ge and Si. Structural features of grain boundaries have been obtained from the direct imaging of atomic columns of [110] tilt grain boundaries in Ge and Si, and more information about actual atomic positions has been obtained from the comparison of high-resolution images with computer simulated images [8, 9, 12–16].

For grain boundaries in materials with a sphalerite structure, there are two kinds of atomic arrangements corresponding to each grain boundary in diamond-structure materials [17, 18]. These depend on the relative positions of higher and lower valence elements. In order to characterize the atomic structure of grain boundaries in compound semiconductors, it is essential to identify the relative positions of the lower and higher valence atoms in high-resolution images. The determination of polarity in GaAs crystals has been carried out successfully by a CBED technique [19, 20], and this technique has been utilized in the study of grain boundaries in GaAs. The species of atoms at atomic sites near the grain boundaries has been identified from a determination of the polarities of the grains on either side of the boundaries.

In this study, systematic investigation has been carried out on the structure of $\Sigma = 19$, [110] grain boundaries in GaAs, which have been grown using the epitaxial thin film deposition techniques. The structural

* Author to whom all correspondence should be addressed.

features like faceting behavior, atomic arrangements, lattice translation, and atomic relaxation of the $\Sigma = 19$, [110] tilt grain boundaries were investigated by TEM.

2. Experimental

2.1. Bicrystal preparation

Ge bicrystals were grown by Czochralski method using a double-seed holder with two single-crystal seeds

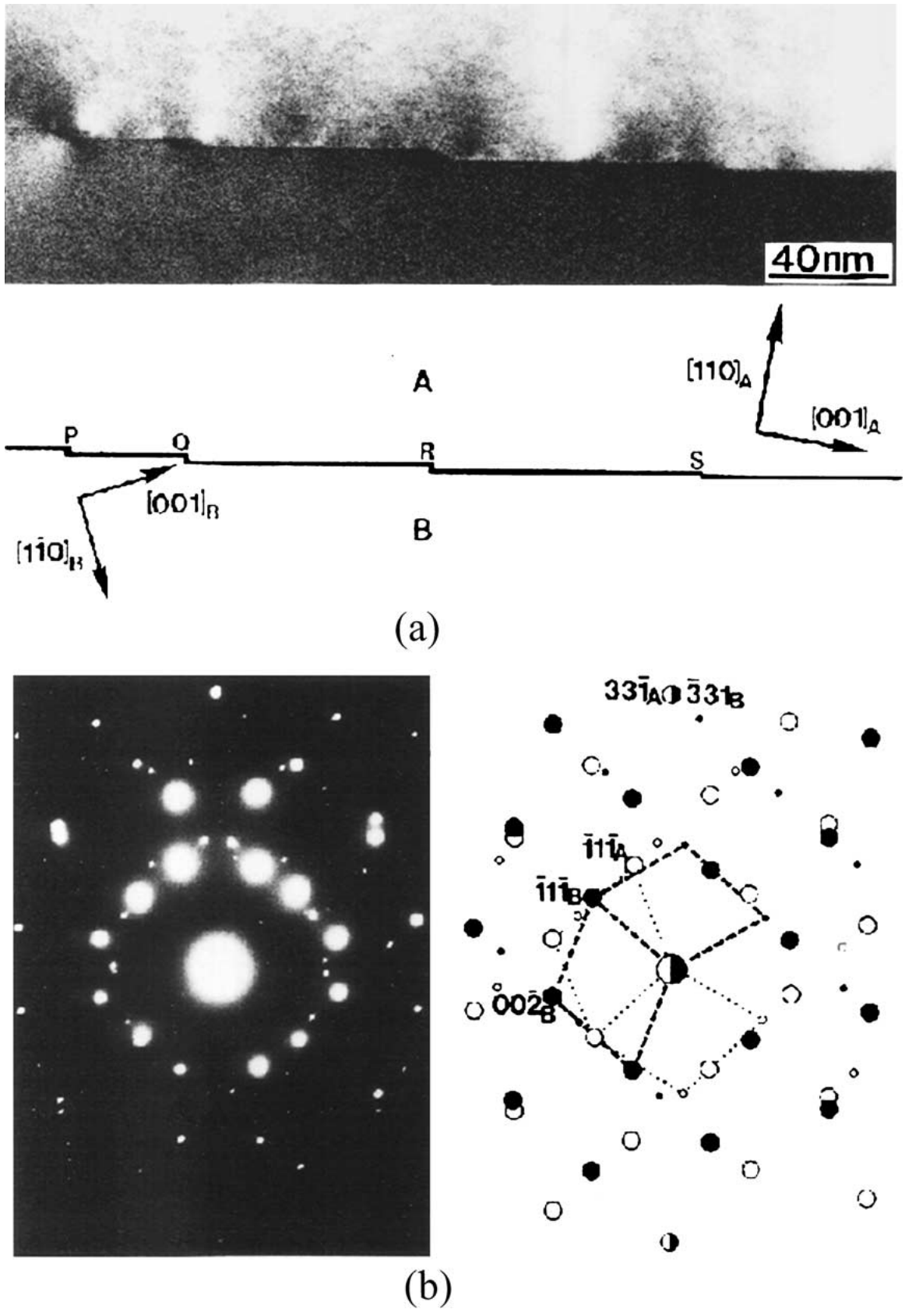

Figure 1 (a) Bright-field image of a $\Sigma = 19$, [110] tilt grain boundary. The boundary appears to facet parallel to $(\bar{3}3\bar{1})_A/(3\bar{3}\bar{1})_B$. (b) Selected-area diffraction pattern corresponding to the area shown in (a). Large open and closed circles correspond to grain A and grain B while small open and closed circles come from microtwins in grain A and grain B. Reflection $\bar{3}3\bar{1}$ from grain A coincide with reflection $\bar{3}31$ from grain B.

of Ge. Substrates of Ge bicrystal were obtained in the following way. Ge bicrystals were cut such that the cutting plane was perpendicular to the grain boundary. The surface of Ge substrates was polished mechanically using diamond powder. The surface was then cleaned by sequentially boiling in acetone and methanol for 6 min each, and then rinsing in de-ionized water for 2 min. The surface was chemically polished in a solution of HF in water and dried in N_2 gas.

GaAs epilayers were grown by organometallic vapor-phase epitaxy (OMVPE) methods. The GaAs growth rate was 60 nm/min, the chamber pressure was 76 Torr, and the As/Ga ratio was 120. The thickness of GaAs epilayers was about 1 μm.

2.2. TEM specimen preparation

Flat-on TEM specimens were prepared in the following manner.

1. 3-mm diameter discs were cut from the boundary region.
2. The Ge side of these discs was polished mechanically to give a total thickness of about 40–50 μm at the disc center.
3. Copper rings were glued to the top and bottom of the thinned samples to support the brittle GaAs bicrystals.
4. The Ge-side of these samples was then ion-milled with Ar^+ until a small hole appeared.

2.3. TEM imaging condition

A JEOL 200 CX operating at 200 kV was used to record the diffraction image as well as selected area diffraction patterns (SADP) corresponding to boundary areas. A JEOL 4000 EX was used to record high-resolution TEM images of tilt grain boundaries. The spherical aberration constant of this microscope (Cs) is 1.0 mm at 400 kV. The electron beam was aligned parallel to the misorientation axis of both grains, the [110] for instance. Diffraction patterns were used to check the tilt condition of the specimens. The $\langle 111 \rangle$ and $\langle 220 \rangle$ diffraction spots from the grains on either side of the tilt grain boundaries must be of the same intensity for the [110] misorientation axis, when the electron beam is parallel to the [110] axis.

The size of the objective aperture was chosen such that the diameter was slightly larger than the spatial frequency of 220 reflections. Considering the contrast transfer function (CTF) calculated for this microscope operating at 400 kV, high-resolution TEM images recorded with defocus values of 40–75 nm were obtained by scattered beams corresponding to the first-band of the CTF. Fourier image processing of the original micrographs of the tilt grain boundaries was carried out in order to remove the effect of the large-angle scattered electrons on the high-resolution images of grain boundaries.

3. Results

A bright-field image of a $\Sigma = 19$, [110] tilt grain boundary is shown in Fig. 1a. A facet appears to lie parallel to the crystallographic plane of $(\bar{3}3\bar{1})_A/(3\bar{3}\bar{1})_B$. Along the facet, bright spots are arrayed about 1.5 nm apart. Steps are observed at P, Q, R and S, and a slightly darker contrast is seen at these sites. The step height measured to be about 3 nm. A selected-area diffraction pattern

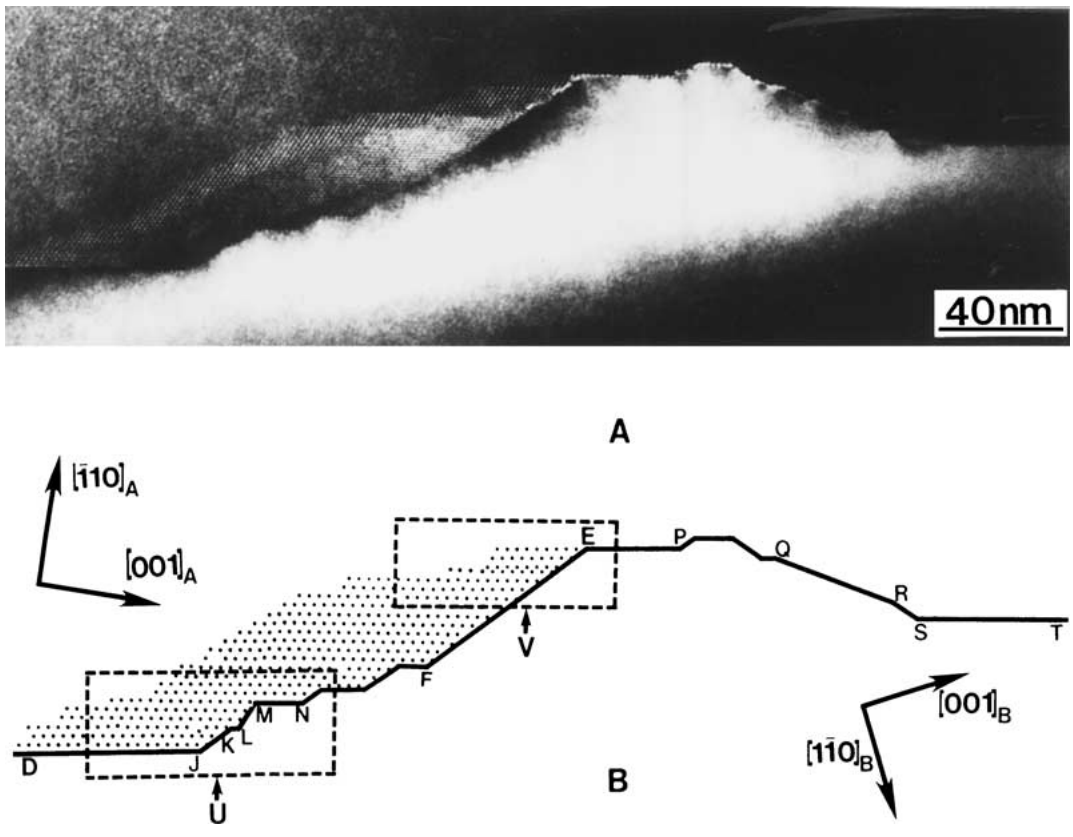

Figure 2 A {331} bright-field image of $\Sigma = 19$, [110] tilt grain boundaries. $(\bar{3}3\bar{1})_A/(3\bar{3}\bar{1})_B$, $(\bar{2}2\bar{7})_A/(4\bar{4}\bar{5})_B$, $(\bar{5}58)_A/(7\bar{7}4)_B$ and $(\bar{2}2\bar{1})_A/(13\bar{1}32)_B$ are seen at DJ, LM, FE and QR, respectively.

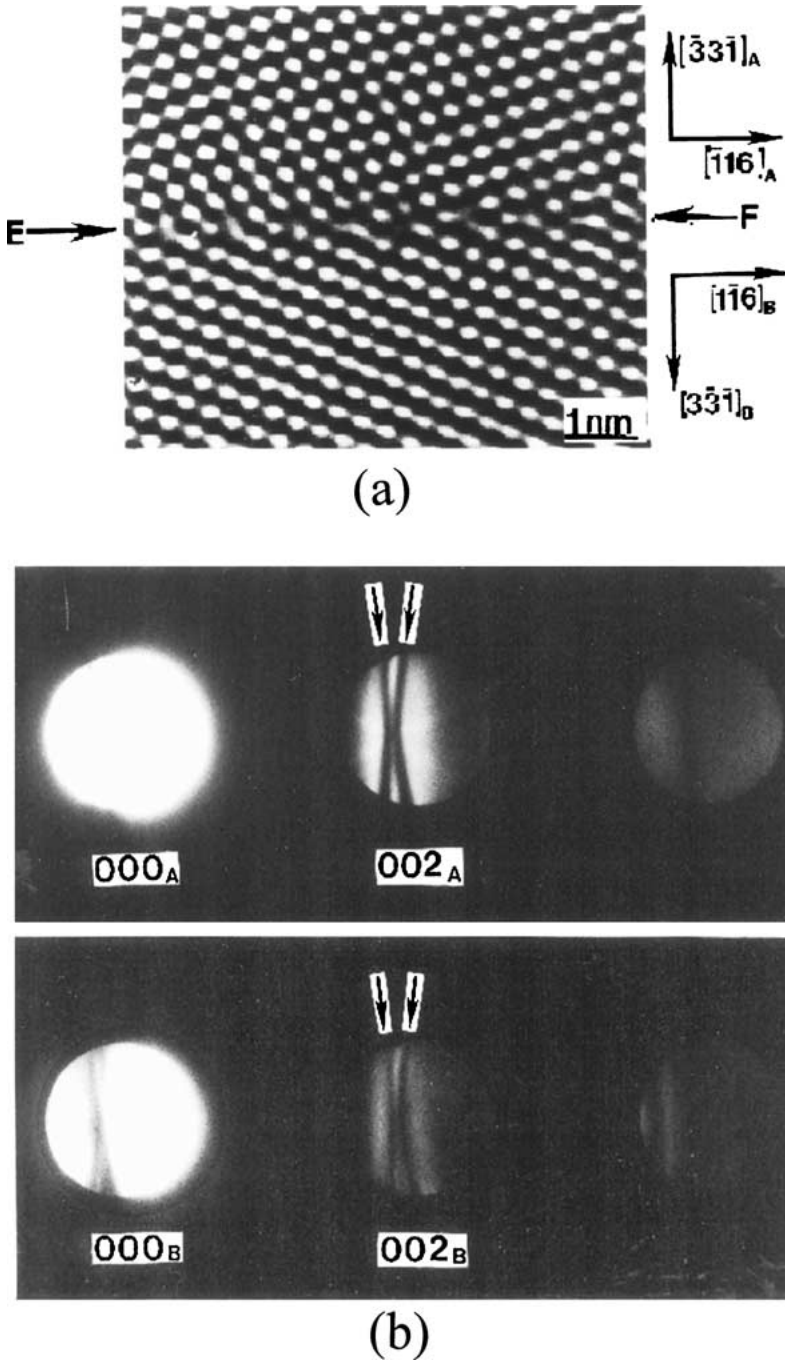

Figure 3 (a) High-resolution image of a $\Sigma = 19$, [110] tilt grain boundary. Bright spots are seen symmetric across the boundary, and a step is shown between T and U. (b) Effect of FOLZ reflections on (200) beams in grain A and grain B is seen in 002_A and 002_B convergent beam disks.

shown in Fig. 1b was recorded at the area shown in Fig. 1a. Four different sets of [110] diffraction patterns are shown in the micrograph. Open and closed large circles correspond to grain A and grain B in the schematic. Reflection $\bar{3}3\bar{1}_A$ is observed to coincide with reflection $\bar{3}31_B$. Diffraction spots of microtwins are also seen and small open and closed circles, in the schematic, represent those from grain A and grain B. The misorientation angle between grain A and grain B is that of $\Sigma = 19$ coincidence.

Fig. 2 shows the strong tendency of a $\Sigma = 19$, [110] tilt grain boundary to facet parallel to particular crystallographic planes. In addition to the $(\bar{3}3\bar{1})_A/(3\bar{3}\bar{1})_B$, $(\bar{2}2\bar{7})_A/(4\bar{4}5)_B$, $(\bar{5}58)_A/(7\bar{7}4)_B$, and $(\bar{2}2\bar{1})_A/(13\bar{1}32)_B$ are seen at DJ, LM, FE and QR, respectively. Relatively short facets are observed to be connected to the $(\bar{3}3\bar{1})/(3\bar{3}\bar{1})$ boundary (DJ) in the area indicated by U. Moiré type contrast appears at the region corresponding to the boundary inclined to the [110] misorientation axis. This boundary is also observed to facet parallel to {331} planes in addition to (110) twist boundary plane. This facet is clearly seen in the area represented by U and V.

In Fig. 3a, a high-resolution image of a $\Sigma = 19$, $(\bar{3}3\bar{1})_A/(3\bar{3}\bar{1})_B$ [110] tilt grain boundary is shown. The {111} lattice images in grain A and grain B indicate that the rotation angle between the two grains is about 26.5°; this misorientation corresponds to that of the $\Sigma = 19$ coincidence for two [110] fcc lattices. The arrangement of bright spots is symmetric across the boundaries. Along the boundaries ST and UV, bright spots form an array of symmetric triangular configurations. A step

with the height of 2a/19[331] is observed between two boundary segments ST and UV. The repeating unit is destroyed between T and U.

In Fig. 3b, the effect of FOLZ reflections on (200) beams in grain A and grain B is shown in 002_A and 002_B convergent beam disks. The determination of the polarity in grain A and followed by the determination in grain B under the same diffraction condition, after rotating the grain by the misorientation angle (26.5°). The polarities determined for each grain on either side of the boundary also indicate that the misorientation angle is 26.5°.

4. Discussion

The strong tendency of a $\Sigma = 19$, [110] tilt grain boundary to facet parallel to particular planes has been seen; the observed facets lie along $(\bar{3}3\bar{1})/(3\bar{3}\bar{1})$, $(\bar{5}58)/(7\bar{7}4)$ and $(\bar{2}2\bar{7})/(4\bar{4}5)$. Fig. 4 shows a [110] projection of two GaAs crystals when one crystal is rotated with respect to the other about [110] axis by 26.5°, which corresponds to the misorientation angle of a $\Sigma = 19$ coincidence. Ga and As sites are represented by triangles and open circles, respectively, while in crystal B, Ga and As are denoted by '+'s and '×'s, respectively. Mirror planes are observed along $(\bar{3}3\bar{1})$ crystallographic planes. {331} and {116} planes appear to contain the highest and second highest densities of coincidence sites and $(\bar{5}58)/(7\bar{7}4)$ is also shown to contain a relatively high density of coincidence sites [21–23]. The $(3\bar{3}\bar{1})/(3\bar{3}1)$ and $(7\bar{7}4)/(5\bar{5}8)$ are observed to be preferred facets for the boundary. These two boundary planes are those planes which have a high planar density of coincidence sites, while no presence of a facet $(\bar{1}1\bar{6})/(1\bar{1}\bar{6})$ has been observed.

The observed step height is 3 nm, which closely matches the distance (3.1 nm) represented by arrow

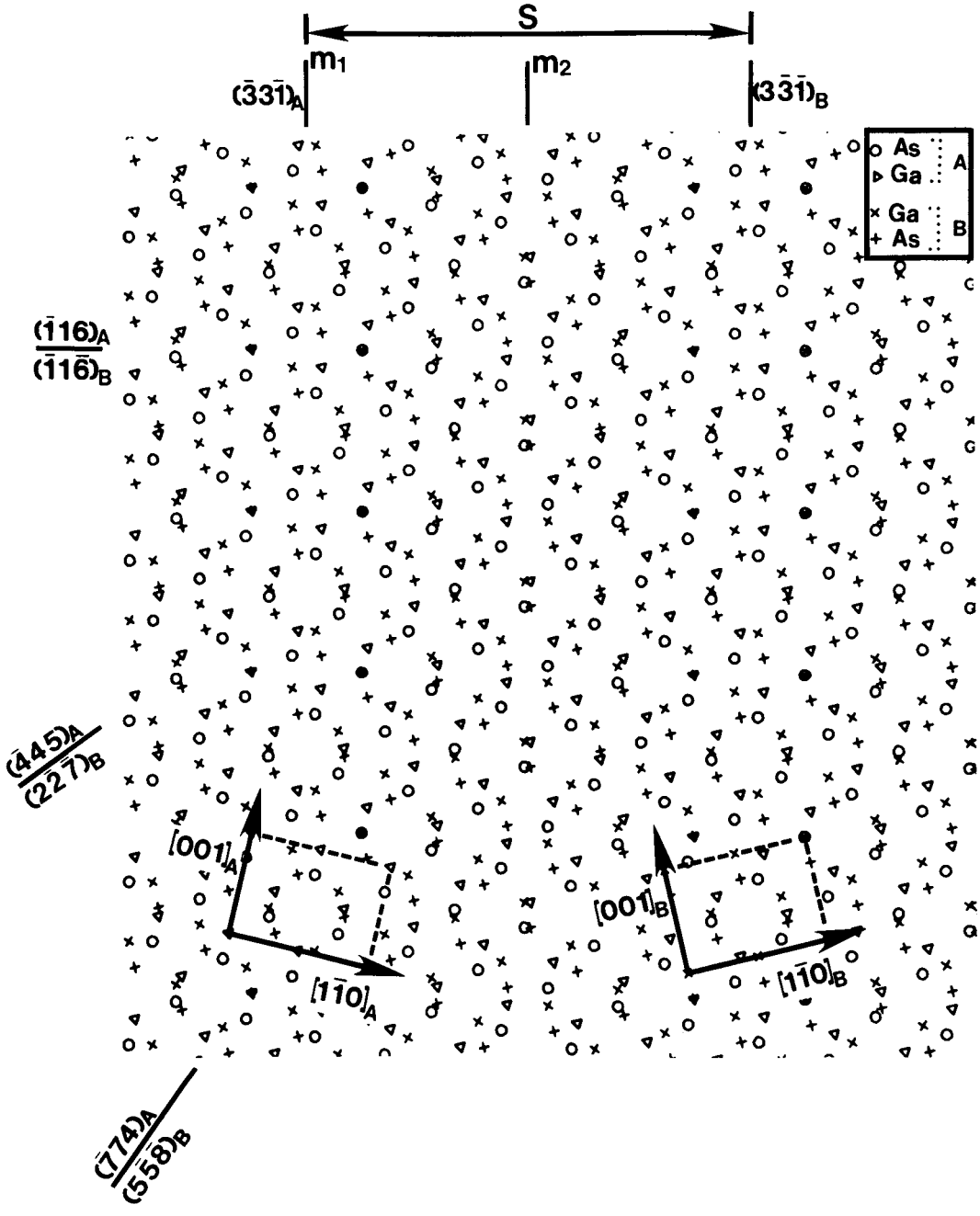

Figure 4 A [110] projection of two GaAs crystals. One crystal is rotated by 26.5° with respect to the other about a [110] common axis. Ga and As sites are represented by triangles and open circles respectively in one crystal, while in the other crystal, they are denoted by '+' and '×', respectively.

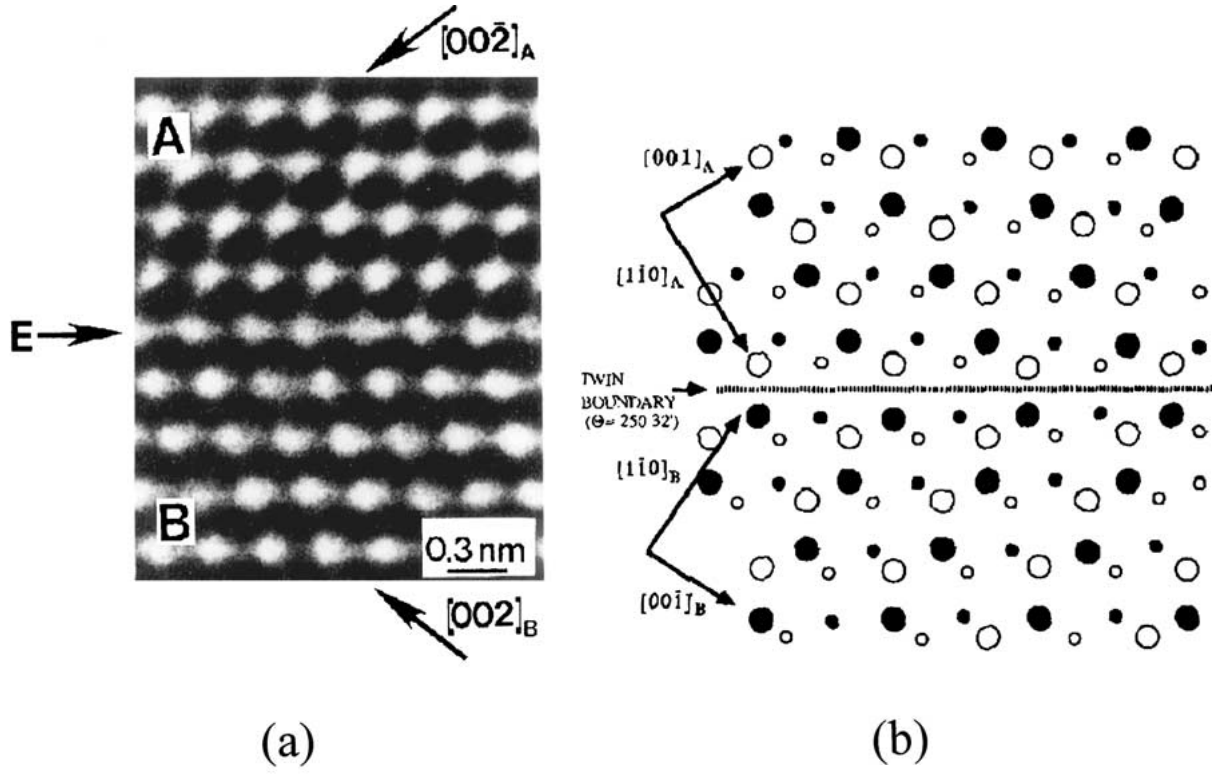

Figure 5 (a) High-resolution image of a coherent twin boundary. A mirror plane is seen along the line indicated by arrow E. Bright spots are arrayed along this plane. (b) [110] projection of atomic arrangements corresponding to a coherent twin boundary in GaAs. Ga and As atoms are represented by open and closed circles respectively, and the two different sizes of circles indicate the two different heights in the [110] projection of a GaAs crystal. The coherent twin boundary plane is indicated by an arrow.

S between two {331} coincidence planes in Fig. 4. This also indirectly indicates that the boundary plane lies right at the {331} mirror plane with a high density of coincidence sites. The appearance of bright spots at the boundary is considered to result from the periodic nature in the structure of this boundary.

The fringe images shown in the twist type boundary are expected to be produced due to double diffraction at the lower grain. When this image pattern was recorded, the imaging condition was such that a 220_A reflection was also excited in addition to the coincidence reflection of 331. If the 220_A reflection is diffracted in the upper grain and then goes into the lower grain as an incident beam; some of the diffracted beam is very close to the original incident beam and the distance is about 1.5 nm^{-1}. This distance is short enough to be included in the objective lens aperture. This beam could therefore interfere with the incident beam to produce the observed fringe images.

The presence of a boundary inclined to the misorientation axis is considered to occur due to the difference in the growth rate locally. It is interesting to note that steps are located at the areas indicated with U and V in Fig. 4. The appearance of steps indicates that the inclination of this boundary is dissociated to produce facets along {331} and {110} planes. Absence of contrast with respect to height along the beam direction in region U and V suggests that the twist type boundary is parallel to {110} plane.

Image simulation has been carried out for perfect GaAs crystals with a [110] orientation under a wide range of thicknesses and defocus values [20]. With the thickness less than 5 nm, the [110] channels appear as bright spots under the defocus values of −40 nm–−70 nm. Such bright spots are arrayed along the mirror plane of coherent twin boundaries in the high-resolution images recorded in this study, as shown in Fig. 5. The shortest distance between Ga and As in the [110] projection is 0.14 nm. These two atomic columns appear as one spot in the high-resolution images because the distance is too short to be resolved by the microscope. Therefore, the image of the mirror plane of the coherent twin boundaries in particular of microtwins in grains can be used to obtain the information about the correspondence of image spots with atomic sites.

The high-resolution image shown in Fig. 6a was obtained by Fourier-image filtering the original high-resolution image in Fig. 3. The relative Ga and As atomic sites were then superimposed on each dark spot. No lattice translation is observed either along the boundary or normal to the boundary plane (perpendicular to the electron beam direction); the arrangements of bright spots on either side of the boundary appear to be symmetric and an extension of each lattice produces an array of coincidence lattice site points such as the atomic sites S and M within the structural unit indicated by the arrow in Fig. 6b. The spacing between the first and the second {331} atomic planes from the boundary plane is about 40% less than normal spacing. However, normal spacing is seen in the third {331} atomic plane from the boundary plane. A model for the atomic structure of this boundary which is consistent with the image is shown in Fig. 6b.

The atoms near the boundary plane (for example, at site S-M in Fig. 6b) appear to form a symmetric configuration occupying the coincidence sites along

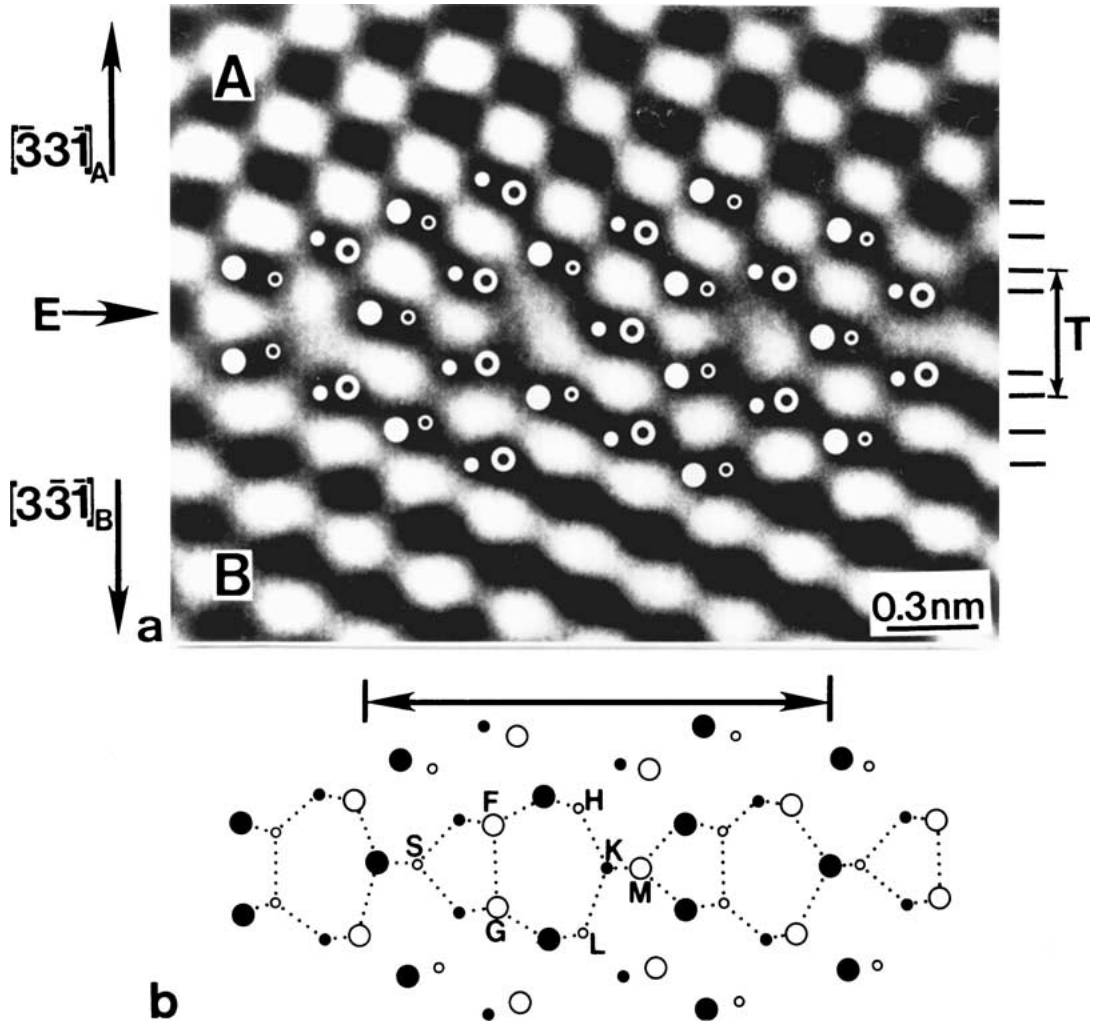

Figure 6 (a) Atomic sites are superimposed on dark spots. Polarities in grains A and B were determined by CBED techniques. The boundary plane is indicated by arrow E. (b) The structural unit of this boundary is seen in the area indicated by an arrow between two bars. A Ga-Ga anti-site bond is present between atomic sites F and G.

the boundary. No dangling bonds are present at this boundary. Anti-site type bonds (Ga-Ga) are observed between the atom site F and G. The length of this anti-site type bond is 0.25 nm; this value is close to the equilibrium bond length between Ga-Ga in solid Ga (orthorhombic). The corresponding bond length in an unrelaxed model structure of this boundary in GaAs is about 0.2 nm.

The translation of atomic sites F and G results from a strong repulsion between two atoms separated by a distance shorter than the normal bond length. Such a change of cross-boundary bond length then enables the bonds to obtain a normal bond length, generating local atom relaxation. However, the relaxation appears to be localized within the first and second atomic planes from the boundary; this region is indicated by arrow T in Fig. 6a.

A structural model has been suggested for this boundary in materials with a diamond structure. The atomic structure of this boundary appears to be similar to that of an a/2[110] edge dislocation core which was suggested by Hornstra. The observation of the atomic structure of this boundary is part of the evidence that there is no dangling bond in the a/2[110] edge dislocation core (between atomic sites F and G in Fig. 6b). A similar local relaxation near this boundary plane was also observed in a similar boundary in Au thin films and Ge [2, 3, 5].

5. Conclusion

Examination of the boundary planes indicates that grain boundaries in GaAs tend to facet parallel to particular crystallographic planes. Since the GaAs epilayers were grown on substrates which were at a relatively high temperature (670°C), the atoms are expected to be very mobile. Since high-temperature kinetics is involved, boundaries of energetically stable forms are highly likely to be present between two grains under the given misorientation. The planar density of coincidence sites appears to be higher along the observed boundary planes. The energy associated with the presence of boundaries is believed to be reduced when the boundaries lie along planes which have a high density of coincidence sites; boundaries are considered to facet parallel to these planes in order to attain a lower energy state. The measured step height is also strongly related to the tendency of the boundary to lie along particular planes with a high density of coincidence sites.

Symmetric $\Sigma = 19\ (3\bar{3}\bar{1})_A/(3\bar{3}1)_B$ [110] boundaries in GaAs appear to achieve lower energy states by significant local atomic relaxation near the boundaries. The

observed structural unit for this boundary consists of one of the symmetric combinations of 5- and 7-member rings, which is similar to the core structure of a/2[110] edge dislocations. The polarities in each grain on either side of the tilt boundaries have been confirmed by direct CBED methods. The result indicates that a lower number of anti-site type bonds occur along the boundaries compared to when the polarity of one grain is reversed. The relaxation results in a more open atomic structure at the boundary, shortening the distance between the first and the second {331} atomic planes from the boundary plane by 40%. The occurrence of the 7-member rings and the relaxation process of this arrangement result in a relatively 'open' atomic structure along the boundaries. The presence of anti-site type bonds between the 5- and the 7-member rings is also expected to cause these tilt boundaries to have a more open atomic structure.

References

1. J. A. KOHN, *Am. Miner.* **43** (1958) 263.
2. J. HORNSTRA, *Physica* **25** (1959) 409.
3. W. KRAKOW, J. T. WETZEL and D. A. SMITH, *Phil. Mag. A* **53** (1986) 739.
4. C. B. CARTER, *Mater. Res. Soc. Symp. Proc.* **5** (1982) 33.
5. R. C. POND, D. A. SMITH and V. VITEK, *Acta Metall.* **27** (1979) 235.
6. D. A. SMITH, V. VITEK and R. C. POND, *ibid.* **25** (1976) 475.
7. G. HASSON, J. Y. BOOS, I. HERBEUVAL, M. BISCONDI and C. GOUX, *Surf. Sci.* **32** (1972) 115.
8. C. D'ANTERROCHES and A. BOURRET, *Phil. Mag. A* **49** (1984) 783.
9. Z. ELGAT, PhD thesis, Cornell University, 1985.
10. J. P. SALERNO, B. W. McCLELLAND, P. VOHL, J. C. C. FAN, W. MACROPOULOS and C. O. BOZKR, *Mater. Res. Soc. Symp. Proc.* **5** (1982) 77.
11. N.-H. CHO, C. B. CARTER, Z. ELGAT and D. K. WAGNER, *Appl. Phys. Lett.* **49** (1986) 29.
12. O. L. KRIVANEK, S. ISODA and K. KOBAYASHI, *Phil. Mag.* **36** (1977) 931.
13. J. C. H. SPENCE, M. A. O'KEEFE and H. KOLAR, *Optik* **49** (1977) 307.
14. R. W. GLAISHER and A. E. C. SPARGO, *Ultramicroscopy* **18** (1985) 323.
15. C. B. CARTER, H. FOLL, D. G. AST and S. L. SASS, *Phil. Mag. A* **43** (1981) 441.
16. W. SKROTZKI, H. WENDT, C. B. CARTER and D. L. KOHLSTEDT, *ibid.* **57** (1988) 383.
17. D. B. HOLT, *J. Phys. Chem. Solids* **25** (1964) 1385.
18. *Idem.*, *ibid.* **23** (1962) 1353.
19. J. TAFTO and J. C. SPENCE, *J. Appl. Cryst.* **15** (1982) 60.
20. B. C. DECOOMAN, PhD thesis, Cornell University, 1987.
21. D. G. BRANDON, *Acta Metall.* **14** (1966) 1479.
22. W. BOLLMANN, *Phil. Mag.* **16** (1967) 363.
23. M. L. KRONBERG and F. H. WILSON, *Trans. AIME* **185** (1949) 501.

Received 4 May 2000
and accepted 13 April 2001